

Validation of a Deforming Grid Method for Unsteady Ground Effect Simulations

Breno Moura Castro

Instituto de Aeronáutica e Espaço - IAE
Praça Mal. Eduardo Gomes, 50 - Jd. das Acácias
CEP: 12228-901 São José dos Campos - SP - Brazil
bmcastro@directnet.com.br

Abstract. Euler computations were carried out to validate a deforming grid method for unsteady ground effect simulations. Two tests were performed for a NACA 0014 airfoil oscillating in pure-plunge motion. The first considered the airfoil in free air. The second test involved the oscillation of the profile close to the ground. The simulations were run for reduced frequencies of $k = 0.5$ and amplitudes of $0.4c$. For the ground-effect case, the mean distance to the ground plane was $0.7c$. A four-block and a three-block grid were used to perform the first and the second tests, respectively. Despite the large deformations of the grids, the present method yielded results for the aerodynamic coefficients in good agreement with a non-deforming-grid solution and an unsteady potential flow solver.

keywords: Euler simulation, unsteady flow, deforming grid, ground effect, flapping propulsion.

1. Introduction

The estimation of the aerodynamic characteristics of oscillating airfoils near the ground, considering viscous effects, requires the use of numerical techniques. The numerical schemes, known generally as Computational Fluid Dynamics (CFD), on their turn, demand a computational grid to discretize the flow-field.

For oscillating airfoils near the ground, an additional feature is required. The computational grid must be adjusted at each time step to accommodate the relative movement between the airfoil and the ground. It is known (Castro, 2001) that the ground effect can enhance the efficiency of thrust generation by means of flapping airfoils.

It has been shown (Jones and Platzer, 1999) that the best efficiency for pure plunge motions is achieved for large amplitude oscillations. Therefore, large deformations of the grid can be expected for simulations of practical thrust generation machines taking advantage of the ground effect. Furthermore, a numerical solver for the prediction of the thrust characteristics must be able to deal with these large deformations with negligible numerical errors.

This work is carried out to evaluate the performance of the NSTRANS code, developed by Platzer and co-workers, to deal with deforming grids. The problem under investigation considers a NACA 0014 airfoil oscillating in pure plunge motion at a mean distance of $0.7c$ of the ground and an amplitude of $0.4c$, where c is the chord of the airfoil. At its lowest position, the airfoil is only $0.3c$ away from the ground. At the highest position, the distance is $1.1c$. This implies large deformations on the grid. The adjustment of the grid at each time step is made with the aid of an algebraic solver embedded in the main computational code. The tests were performed for a reduced frequency of 0.5 and for Mach numbers of 0.2 and 0.3 .

The results of this method were compared with the ones obtained by an unsteady panel method called USPOT and show good agreement for lift and drag coefficients. Some Mach number dependency for the amplitude of the thrust coefficient was observed.

2. Theoretical Background

2.1. Governing Equations

The solution for the problem of an unsteady, compressible, and inviscid flow is obtained by solving the Euler equations. They are presented in matrix, non-dimensional, and curvilinear coordinate form in Eq. (1):

$$\partial_\tau \hat{Q} + \partial_\xi \hat{F} + \partial_\zeta \hat{G} = 0 \quad (1)$$

where $Q = (\rho, \rho u, \rho w, e)^T$ is the dependent variable, representing a vector which components are the flow state variables, and $\hat{Q} = J^{-1}Q$. The Jacobian of the coordinate transformation from the system (x, y, t) to (ξ, ζ, τ) is $J = (x_\xi z_\zeta - x_\zeta z_\xi)^{-1}$.

The reference values for non-dimensionalization are the chord length c , the free stream density ρ_∞ , the free stream speed-of-sound a_∞ , the time c/a_∞ , and the specific energy $\rho_\infty a_\infty^2$.

\hat{F} and \hat{G} are the inviscid flux vectors:

$$\hat{F} = J^{-1} \begin{Bmatrix} \rho U \\ \rho u U + \xi_x p \\ \rho w U + \xi_z p \\ (e + p)U - \xi_t p \end{Bmatrix} \quad \hat{G} = J^{-1} \begin{Bmatrix} \rho W \\ \rho u W + \zeta_x p \\ \rho w W + \zeta_z p \\ (e + p)W - \zeta_t p \end{Bmatrix} \quad (2)$$

where:

$$\begin{aligned} \hat{\xi}_t &= J^{-1} \xi_t = x_\zeta z_\tau - x_\tau z_\zeta & \hat{\zeta}_t &= J^{-1} \zeta_t = x_\tau z_\xi - x_\xi z_\tau \\ \hat{\xi}_x &= J^{-1} \xi_x = z_\zeta & \hat{\zeta}_x &= J^{-1} \zeta_x = -z_\xi \\ \hat{\xi}_z &= J^{-1} \xi_z = -x_\zeta & \hat{\zeta}_z &= J^{-1} \zeta_z = x_\xi \end{aligned} \quad (3)$$

The terms U and W are the contravariant velocity components given by:

$$\begin{aligned} U &= \xi_t + \xi_x u + \xi_z w \\ W &= \zeta_t + \zeta_x u + \zeta_z w \end{aligned} \quad (4)$$

Pressure is related to the other variables through the equation of state for an ideal gas:

$$p = (\gamma - 1) [e - \rho(u^2 + w^2)/2] \quad (5)$$

2.2. Numerical Technique

The Euler equations are discretized using an alternate direction implicit (ADI), third-order accurate in space, second-order accurate in time, finite-volume scheme, which can be represented by:

$$\begin{aligned} \left[I + h_\xi (\nabla_\xi \hat{A}_{i,k}^+ + \Delta_\xi \hat{A}_{i,k}^-)^p \right] \Delta \hat{Q}_{i,k}^* &= -\hat{r}_{i,k}^p \\ \left[I + h_\zeta (\nabla_\zeta \hat{B}_{i,k}^+ + \Delta_\zeta \hat{B}_{i,k}^-) \right] (\hat{Q}_{i,k}^{p+1} - \hat{Q}_{i,k}^p) &= \Delta \hat{Q}_{i,k}^* \end{aligned} \quad (6)$$

where:

$$\hat{r}_{i,k}^p = (\hat{Q}_{i,k}^p - \hat{Q}_{i,k}^n) + h_\xi (\hat{F}_{i+1/2,k} - \hat{F}_{i-1/2,k})^p + h_\zeta (\hat{G}_{i,k+1/2} - \hat{G}_{i,k-1/2})^p \quad (7)$$

The variables \hat{A} and \hat{B} are the flux Jacobian matrices and are defined as $\hat{A} = \partial \hat{F} / \partial \hat{Q}$ and $\hat{B} = \partial \hat{G} / \partial \hat{Q}$, respectively. A flux splitting, according to Steger and Warming (Steger and Warming, 1981), is applied to matrices \hat{A} and \hat{B} , where $\hat{A} = \hat{A}^+ + \hat{A}^-$ and $\hat{B} = \hat{B}^+ + \hat{B}^-$.

The h quantities are defined as $h_\xi = \Delta \tau / \Delta \xi$ and $h_\zeta = \Delta \tau / \Delta \zeta$. ∇ , Δ , and δ are the forward, backward, and central difference operators, respectively.

The variables $\hat{F}_{i+1/2,k}$ and $\hat{G}_{i,k+1/2}$ are numerical fluxes. The superscript $(\cdot)^n$ denotes the physical time step and the superscript $(\cdot)^p$ is related to Newton sub-iterations within each physical time step, which are used to improve time accuracy. These sub-iterations minimize the linearization and factorization errors and help drive the left-hand side of Eq. (6) to zero.

Inviscid numerical fluxes, $\hat{F}_{i+1/2,k}$ and $\hat{G}_{i,k+1/2}$, are evaluated by means of the Osher's third-order accurate, upwind-biased scheme (Chakravarthy and Osher, 1983). Linearization of the left-hand side of Eq. (6) is performed by evaluating the flux Jacobian matrices, \hat{A} and \hat{B} , with the Steger and Warming flux-vector splitting (Steger and Warming, 1981). Furthermore, a Total Variation Diminishing (TVD) flux limiter suggested by Rai and Chakravarthy (Rai and Chakravarthy, 1986) is applied to minimize numerical oscillations at shocks developed at transonic speeds. Grid movement and deformation compatibility is obtained by using the methodology presented by Tamura and Fujii (Tamura and Fujii, 1993).

2.3. Boundary conditions

A special treatment for boundary conditions must be used for the problem under investigation in this work. Because the ground plane is close to the airfoil section, the use of a single-block, C-grid would require a very skewed mesh in the vertical direction. Therefore, a three-block grid approach can be used instead of a single-block grid, as shown in the schematic in Fig. 1. The main block, or block (1), represents the region around the airfoil and also the wake behind it. The second, or block (2), fills the region upstream of the first one. The third, or block (3), completes the domain above the first two blocks.

For inviscid flow solutions, the flow-tangency boundary condition is used at the surface of the airfoil. Density and pressure are extrapolated to the surface. For unsteady motions, the flow-tangency condition is modified to include the

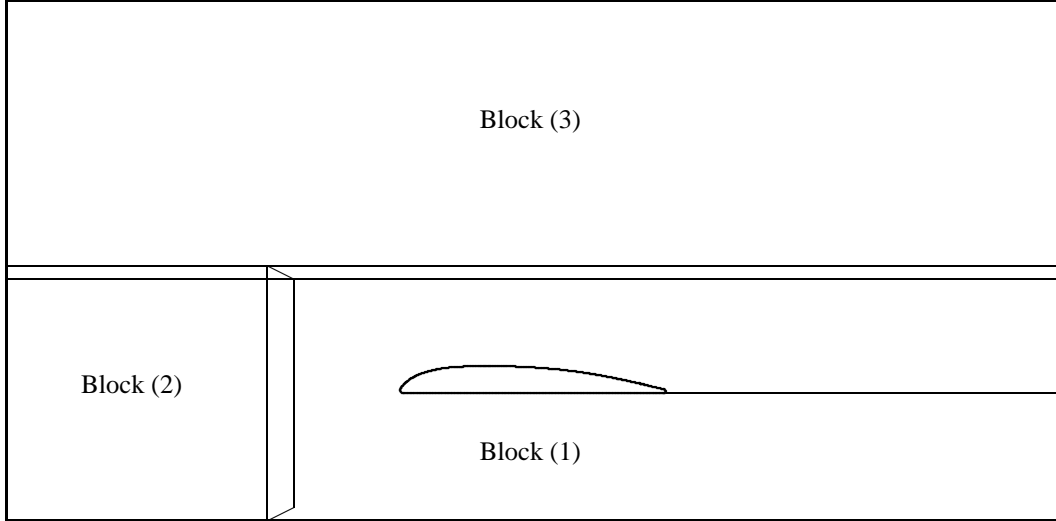


Figure 1: Schematic of the three-block grid for the airfoil-in-ground-effect problem

local motion of the airfoil, which also contributes to the pressure on the surface. Therefore, the momentum equation normal to the surface (ζ direction) is solved to predict the pressure

$$\partial_{\zeta} p|_{wall} = -\frac{1}{\nabla^2 \zeta} \left[\rho \partial_t \left\{ \begin{array}{l} \dot{x}|_{wall} \\ \dot{y}|_{wall} \end{array} \right\} \cdot \nabla \zeta + \partial_{\zeta} \rho|_{wall} \nabla \xi \cdot \nabla \zeta \right] \quad (8)$$

where $\dot{x}|_{wall}$ and $\dot{y}|_{wall}$ are the components of the airfoil velocity. Furthermore, $\nabla \xi \cdot \nabla \zeta = 0$ when assuming that the grid is orthogonal at the surface.

The ground plane is assumed to be a symmetry plane. Therefore, it can be modeled as a solid wall where the symmetry boundary condition is given by Eq. (9).

$$\left[\frac{\partial q}{\partial n} \right]_{wall} = 0 \quad (9)$$

where n represents the normal direction at the wall.

Inflow boundary conditions are applied to the points on the left boundaries of blocks (2) and (3) and also to the upper boundary of block (3). Outflow boundary conditions are specified to the points on the right boundary of blocks (1) and (3).

The boundaries on the left of domain (1) and right of domain (2) are updated by means of an overlapping region. There is an overlapping of the blocks and the flow variables are transferred directly from one domain to the other. The same type of boundary condition is used between blocks (1) and (3), and between (2) and (3). Because of the overlapping regions, direct transfer of the flow variables ($\rho, \rho u, \rho w, e$) can be used.

2.4. Deforming-Grid Compatibility

The Euler equations represented by Eq. (1) are compatible with deforming- and moving-grid problems, as shown in Castro (2001). Theoretically, the Euler equations can handle problems in which both ξ_t and ζ_t are different from zero. Computationally, the numerical scheme must be conservative both in time and space in order to guarantee deforming-grid compatibility.

Thomas and Lombard (Thomas and Lombard, 1979) suggest the use of the Geometric Conservation Law (GCL), Eq. (10), for solving problems involving a changing or deforming grid.

$$\partial_{\tau} (J^{-1}) + (\hat{\xi}_t)_{\xi} + (\hat{\zeta}_t)_{\zeta} = 0 \quad (10)$$

The GCL is analytically satisfied by the unsteady Euler equations written in curvilinear coordinates form. Nonetheless, in order to satisfy the GCL numerically, the metrics associated with computations of the numerical fluxes must be calculated using a conservative scheme. Thomas and Lombard suggest the following conservative scheme for the 3-D metrics:

$$\begin{aligned} \hat{\xi}_x &= (y_{\eta z})_{\zeta} - (y_{\zeta z})_{\eta} & \hat{\eta}_x &= (y_{\zeta z})_{\xi} - (y_{\xi z})_{\zeta} \\ \hat{\zeta}_x &= (y_{\xi z})_{\eta} - (y_{\eta z})_{\xi} & & \text{etc.} \end{aligned} \quad (11)$$

For 2-D metrics, Eq. (11) is reduced to the form presented in Eq. (3) and the scheme is automatically conservative in space. Therefore, the numerical scheme used in the present work is conservative in space. Thomas and Lombard (Thomas and Lombard, 1979) also suggest the inclusion of an extra term in the discretized equations to achieve moving-grid compatibility. According to their approach, the Osher scheme (Chakravarthy and Osher, 1983) would become:

$$\begin{cases} IJ^{-1} + h_{\xi}(\nabla_{\xi}\tilde{A}_{i,k}^+ + \Delta_{\xi}\tilde{A}_{i,k}^-)^p \\ IJ^{-1} + h_{\zeta}(\nabla_{\zeta}\tilde{B}_{i,k}^+ + \Delta_{\zeta}\tilde{B}_{i,k}^-) \end{cases} \Delta Q_{i,k}^* = -r_{i,k}^p \quad (12)$$

$$(Q_{i,k}^{p+1} - Q_{i,k}^p) = IJ^{-1}\Delta Q_{i,k}^*$$

where:

$$r_{i,k}^p = J^{-1}(Q_{i,k}^p - Q_{i,k}^n) + \Delta(J^{-1})Q_{i,k}^n + h_{\xi}(\hat{F}_{i+1/2,k} - \hat{F}_{i-1/2,k})^p + h_{\zeta}(\hat{G}_{i,k+1/2} - \hat{G}_{i,k-1/2})^p \quad (13)$$

Now, the (\cdot) terms represent Jacobians with respect to Q , or $\partial(\cdot)/\partial Q$, instead of \hat{Q} and the term $\Delta(J^{-1})$ is obtained by the GCL:

$$\Delta(J^{-1}) = -\Delta\tau[(\hat{\xi}_t)_{\xi}^n + (\hat{\zeta}_t)_{\zeta}^n] \quad (14)$$

One of the differences between Eq. (12) and Eq. (6) is the way they are solved. The former solves for Q while the latter solves for \hat{Q} . The other difference is the extra term $\Delta(J^{-1})Q_{i,k}^n$ in the RHS of Eq. (12). The presence of this term is due merely to the fact that one of the equations is solved for Q while the other is solved for \hat{Q} . This can be seen by expanding the term $\partial\hat{Q}/\partial\tau$:

$$\frac{\partial\hat{Q}}{\partial\tau} = \frac{\partial(J^{-1}Q)}{\partial\tau} = Q\frac{\partial(J^{-1})}{\partial\tau} + (J^{-1})\frac{\partial Q}{\partial\tau} \quad (15)$$

Writing Eq. (15) in discrete form:

$$\frac{\Delta\hat{Q}}{\Delta\tau} = Q\frac{\Delta(J^{-1})}{\Delta\tau} + (J^{-1})\frac{\Delta Q}{\Delta\tau} \quad (16)$$

Multiplying Eq. (16) by $\Delta\tau$ and using a finite difference approximation:

$$\hat{Q}_{i,k}^p - \hat{Q}_{i,k}^n = Q^n\Delta(J^{-1}) + (J^{-1})^n(Q_{i,k}^p - Q_{i,k}^n) \quad (17)$$

Substituting Eq. (17) into Eq. (7), one obtains Eq. (13), which is the method based on the GCL suggested by Thomas and Lombard. Therefore, Eq. (6) is mathematically equivalent to Eq. (12). In order for them to be numerically equivalent, according to the work of Tamura and Fujii (Tamura and Fujii, 1993), the scheme must also be conservative in time. This feature is achieved by carefully choosing the Jacobian to be used in Eq. (7). They suggest using:

$$(J^{-1})' = \frac{1}{2}[(J^{-1})^n + (J^{-1})^{n+1}] \quad (18)$$

3. Results and Discussion

This section is concerned with two validation tests performed with deforming grids for a NACA 0014 profile submitted to a harmonic pure-plunge motion. The non-dimensional equation of motion is given by:

$$h = \hat{h} \sin(M_{\infty}k\tau) \quad (19)$$

where \hat{h} represents the half amplitude and $k = \omega V_{\infty}/c$ is the reduced frequency of the motion.

3.1. Subsonic Flow Test

This test is designed to demonstrate the ability of this method to perform unsteady computations with a deforming grid for subsonic flow. The problem is the pure plunge oscillation of a NACA 0014 airfoil. The airfoil is moving with a free-stream Mach number $M_{\infty} = 0.3$ and a reduced frequency $k = 0.5$. The half amplitude of the plunge motion is $0.4c$.

First, an unsteady inviscid solution is performed using a single grid around the airfoil. This grid moves along with the airfoil as a solid body. Therefore, the grid is moving but not deforming. The grid used for the computations is a C-grid with 281 points in the ξ direction and 51 in the ζ direction. The single-block grid is shown in Fig. 2.

Second, another solution is computed using a four-block grid. The main block is a C-grid that contains the airfoil. The second block is an H-grid placed just upstream of the main block. The third block is placed right on top of the first two. The fourth block is a mirror image of the third with respect to the chord plane of the airfoil. This grid is shown in Fig. 3. Blocks two, three, and four stay fixed at all times. The only block allowed to deform, in order to accommodate the motion

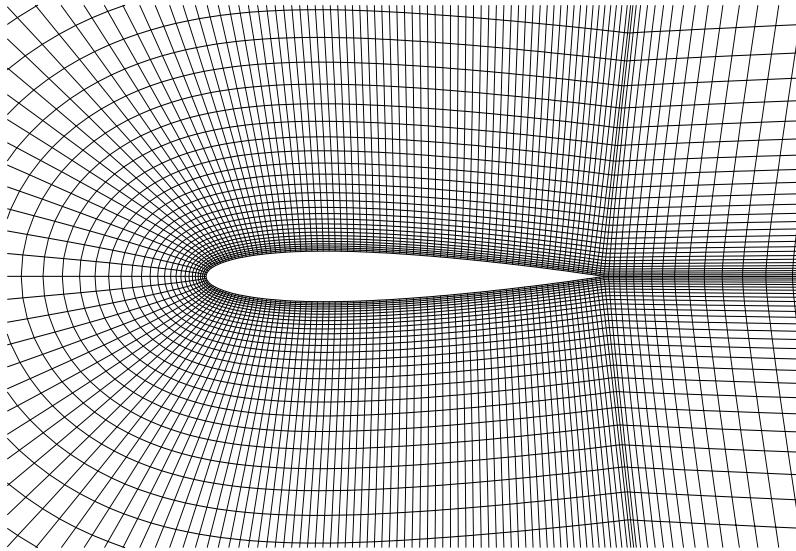


Figure 2: Close-up of the single-block grid around the airfoil

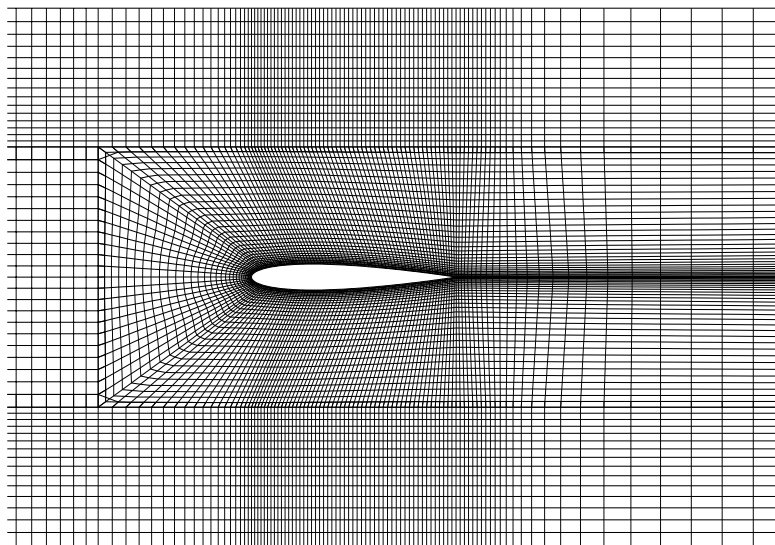


Figure 3: Portion of the four-block grid around the airfoil

of the airfoil, is the main one. The outer boundary of this block stays fixed in order to exchange boundary conditions with the other blocks.

The comparison of the two solutions is shown in Fig. 4. The solution for the single-block grid is represented by the dashed line and the solution for the four-block grid corresponds to the solid line. Despite a very large deformation of the first block in the four-block solution, the agreement with the single-block solution is quite reasonable. The maximum deviations for the lift, drag, and moment coefficients are around 2.1%, 3.5%, and 2.7%, respectively.

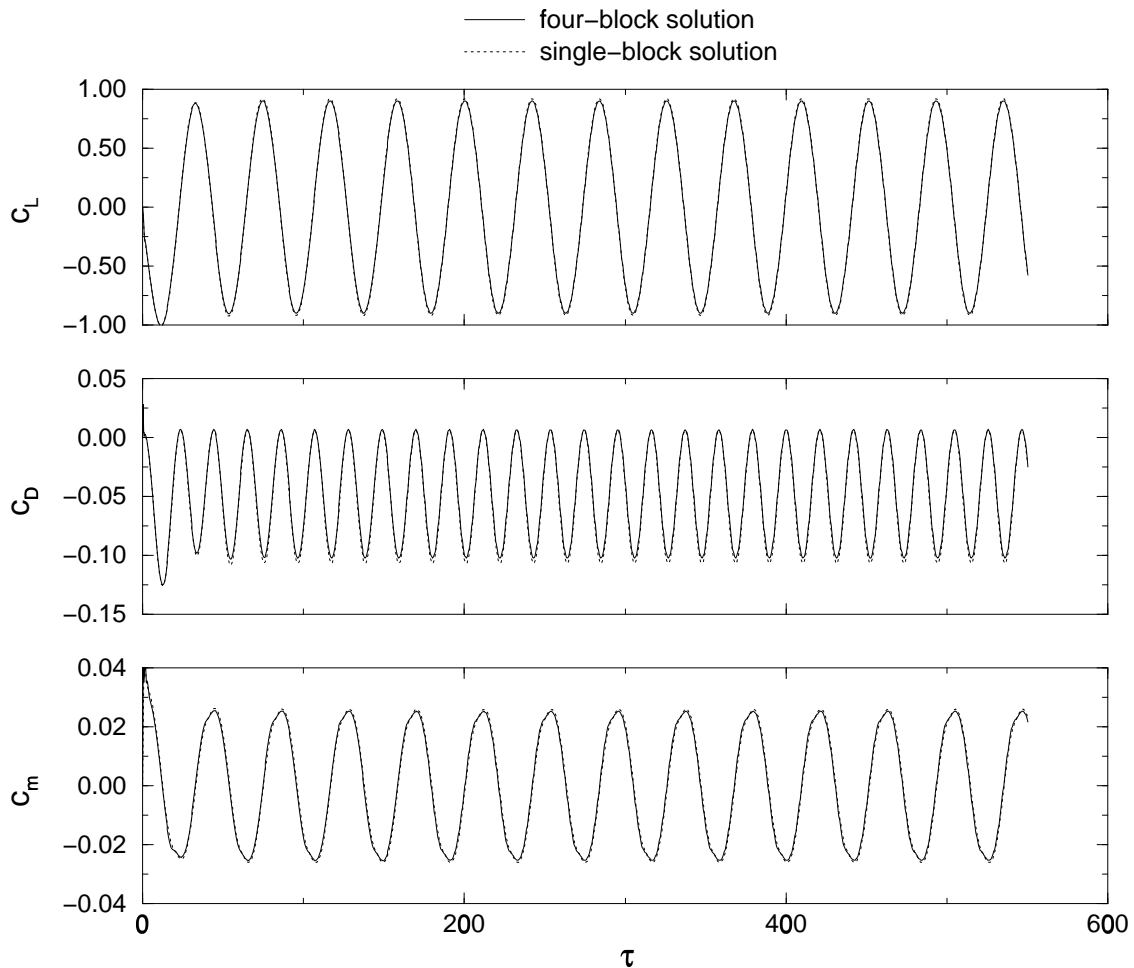


Figure 4: Comparison of Euler solutions for single- and four-block grids

The upper and lower boundaries of the first block for the four-block grid were placed at $h = 0.7$ and $h = -0.7$, respectively. The highest and lowest positions for the airfoil correspond to $h = 0.4$ and $h = -0.4$, respectively. This means that the deformation of the first block is quite large. To better illustrate this point, the four-block grid with the airfoil in its lowest position ($h = -0.4$) is shown in Fig. 5. A steady-state solution for the airfoil at $h = -0.4$ is evaluated and compared to a similar computation for $h = 0$ (undeformed grid) in Fig. 6. The solver is not able to predict a symmetric solution for $h = -0.4$, as it is for $h = 0$, due to the large deformation of the grid. This deviation of the steady-state solution for $h = -0.4$ may explain the difference between the single-block and the four-block solutions for the unsteady problem.

Despite the large deformation of the grid, this method was able to keep the difference between the single-block and the four-block solutions lower than 4%. It is important to note that the four-block grid used here is just an extension of the three-block grid used to solve the airfoil-in-ground-effect problem.

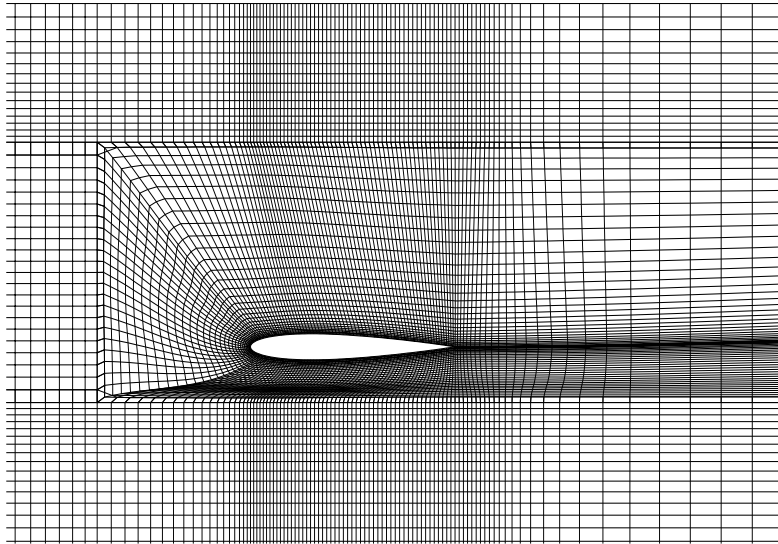


Figure 5: Detail of the four-block grid in its most deformed condition

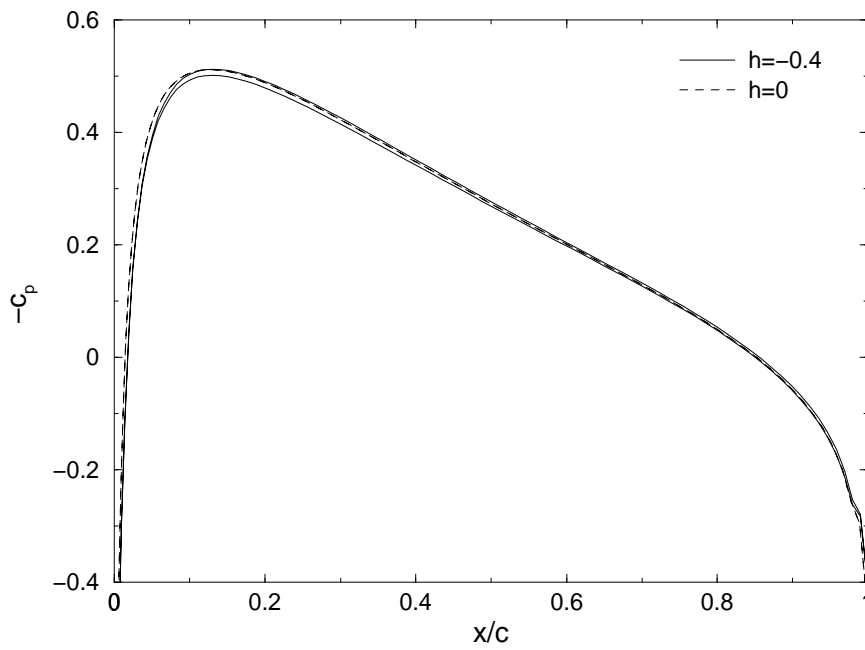


Figure 6: Steady-state pressure distribution for the four-block grid

3.2. Airfoil-in-Ground-Effect and Pure-Plunge Motion

A final validation of the present code is performed for a profile near the ground. This computation shows that the equations for deforming grids can compute the flow over an oscillating airfoil in ground effect accurately.

Euler solutions for a pure plunging NACA 0014 near the ground are compared with the one obtained by using an unsteady potential flow solver called USPOT (Pang, 1988). The reduced frequency of the oscillation is $k = 0.5$. The half amplitude of the motion is $\hat{h} = 0.4$. The distance from the wing at its mean position to the ground plane is $d = 0.7$.

The Euler solutions were run for Mach numbers of $M_\infty = 0.2$ and $M_\infty = 0.3$. The multi-block grid used is shown in Fig. 7. The dimensions for blocks (1), (2), and (3) are 289×41 , 41×39 , and 165×51 , respectively. The solutions for the two Mach numbers are presented in Fig. 8 and compared with the USPOT solution. The incompressible flow solution computed by USPOT corresponds to a Mach number of $M_\infty = 0$. The Euler solutions for $M_\infty = 0.2$ and $M_\infty = 0.3$ show a maximum lift coefficient higher than the one predicted by USPOT. Nonetheless, clearly, the tendency is to approach the incompressible solution as the Mach number diminishes. The same behavior is observed with respect to the drag coefficient. The minimum values for the Euler drag coefficients tend to move toward the USPOT solution as the Mach number decreases.

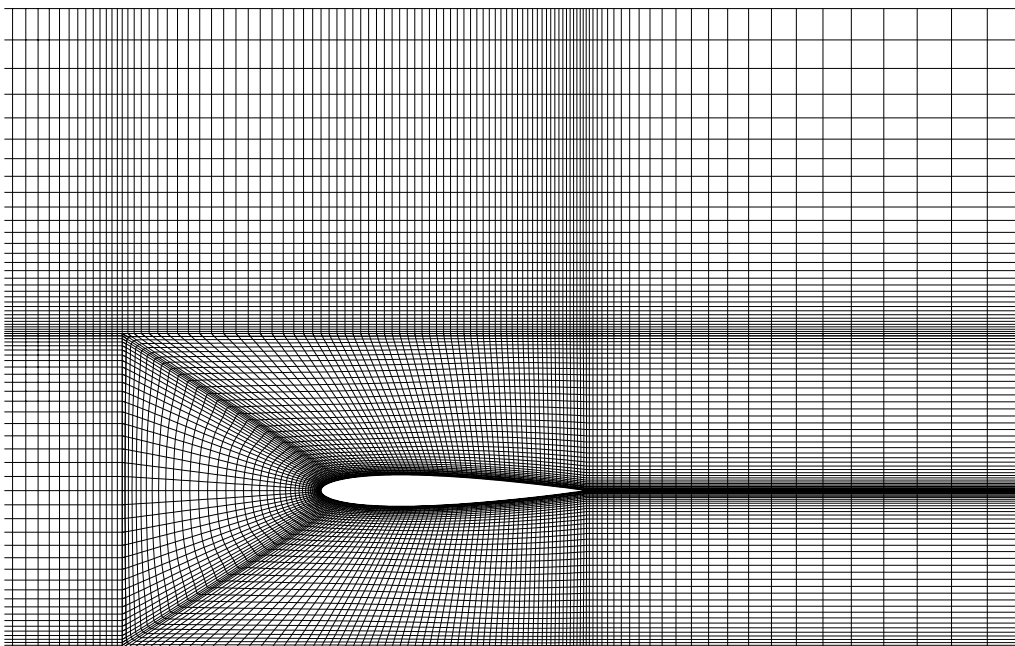


Figure 7: Euler multi-block grid near the airfoil

The influence of the Mach number on the aerodynamic coefficients is known to be quite significant for wings in extreme ground effect (Rozhdestvensky, 2000). For wings in extreme ground effect, meaning distances from the ground lower than 10% of the chord, the aerodynamic coefficients vary with the parameter $(1 - M_\infty^2)^{-1}$ and not $(1 - M_\infty^2)^{-1/2}$. Even though the smallest distance from the airfoil to the ground during the oscillation is $d = 0.3$, the influence of the Mach number is still significant.

This computation shows that the solution obtained with the compressible, deforming-grid code is in good agreement with the solution calculated for the unsteady potential flow. Therefore, the present solver shows that it can perform accurately for a deforming grid situation. Furthermore, the solution shows a significant influence of the Mach number on the unsteady flow characteristics of the airfoil-in-ground-effect configuration.

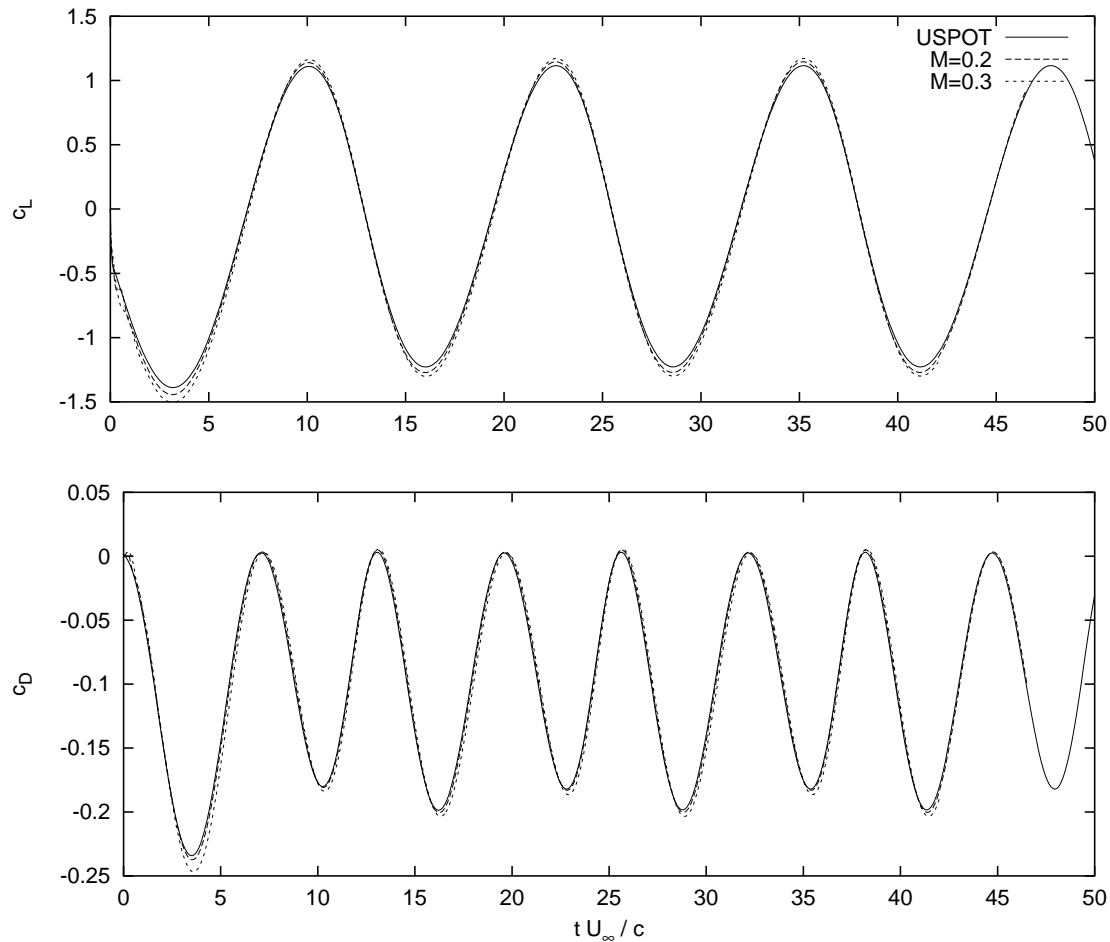


Figure 8: Comparison of Euler and Potential Flow Solutions for a Biplane Configuration

4. Concluding Remarks

Two Euler simulations were performed to validate a deforming grid method for unsteady ground effect calculations. The first test was related with an airfoil oscillating in free air. The second involved a profile in pure-plunge motion near the ground.

The comparison of a four-block, deforming grid simulation with the non-deforming grid solution, for the first test, showed that the present method was able to keep the difference between the two solutions lower than 4%, in spite of the large deformation of the four-block grid.

The second test was performed with a three-block, deforming grid and the results of this method were compared with the ones obtained by an unsteady panel method called USPOT. This computation showed that the solution obtained by the present code is in good agreement with the lift, drag, and moment coefficients calculated for the unsteady potential flow. Some Mach number dependency for the amplitude of the thrust coefficient was observed.

Consequently, the present solver showed that it can perform accurately for deforming grid problems. Nonetheless, further investigation is suggested to explore some parameters such as the reduced frequencies and amplitudes of motion in order to assess the region in which this method yields reliable results.

5. References

- Castro, B. M., 2001, “Multi-Block Parallel Navier-Stokes Simulation of Unsteady Wind Tunnel and Ground Interference Effects”, PhD thesis, Naval Postgraduate School, Monterey, CA.
- Chakravarthy, S. R. and Osher, S., 1983, Numerical Experiments with the Osher Upwind Scheme for the Euler Equations, “AIAA Journal”, Vol. 21, No. 9, pp. 1241–1248.
- Jones, K. D. and Platzer, M. F., 1999, An Experimental and Numerical Investigation of Flapping-Wing Propulsion, 37th AIAA Aerospace Sciences Meeting and Exhibit, Reno, NV.

- Pang, C. K., 1988, "A Computer Code for Unsteady Incompressible Flow past Two Airfoils", Aeronautical Engineer's Thesis, Naval Postgraduate School.
- Rai, M. M. and Chakravarthy, S. R., 1986, An Implicit Form for the Osher Upwind Scheme, "AIAA Journal", Vol. 24, No. 5, pp. 735–743.
- Rozhdestvensky, K. V., 2000, "Aerodynamics of a Lifting System in Extreme Ground Effect", Springer, ISBN 3-540-66277-4.
- Steger, J. L. and Warming, R. F., 1981, Flux Vector Splitting of the Inviscid Gasdynamic Equations with Application to Finite-Difference Methods, "Journal of Computational Physics", Vol. 40, pp. 263–293.
- Tamura, Y. and Fujii, K., 1993, Conservation Law for Moving and Transformed Grids, "AIAA Paper 93-3365", Orlando, FL.
- Thomas, P. D. and Lombard, C. K., 1979, Geometric Conservation Law and Its Application to Flow Computations on Moving Grids, "AIAA Journal", Vol. 17, No. 10, pp. 1030–1037.